Hindawi Publishing Corporation
International Journal of Photoenergy
Volume 2012, Article ID 767054, 12 pages
doi:10.1155/2012/767054

Research Article

TiO_2:(Fe, S) Thin Films Prepared from Complex Precursors by CVD, Physical Chemical Properties, and Photocatalysis

V. G. Bessergenev,[1] M. C. Mateus,[1] D. A. Vasconcelos,[1] J. F. M. L. Mariano,[1] A. M. Botelho do Rego,[2] R. Lange,[3] and E. Burkel[4]

[1] *FCT, Universidade do Algarve, Campus de Gambelas, 8005-117 Faro, Portugal*
[2] *CQFM and IN, IST, Universidade Técnica de Lisboa, 1049-001 Lisboa, Portugal*
[3] *Informatics and Electrotechnics, University of Rostock, 18055 Rostock, Germany*
[4] *Institute of Physics, University of Rostock, 18055 Rostock, Germany*

Correspondence should be addressed to V. G. Bessergenev, vbess@ualg.pt

Received 17 October 2011; Accepted 30 November 2011

Academic Editor: Jiaguo Yu

The TiO_2 thin films were prepared using $Ti(dpm)_2(OPr^i)_2$ and $Ti(OPr^i)_4$ (dpm = 2,2,6,6-tetramethylheptane-3,5-dione, Pr^i = isopropyl) as the precursors. The volatile compounds $Fe[(C_2H_5)_2NCS_2]_3$ and $[(CH_3)C]_2S_2$ were used to prepare doped TiO_2 films. The synthesis was done in vacuum or in the presence of Ar and O_2. The pressure in the CVD chamber was varied between 1.2×10^{-4} mbar and 0.1 mbar, with the system working either in the molecular beam or gas flow regime. Physical, chemical, and photocatalytic properties of the (Fe, S)-doped TiO_2 films were studied. Those TiO_2:(Fe, S) films prepared from the $Ti(OPr^i)_4$ precursor show increased photocatalytic activities, very close to those of Degussa P25 powder in UV region.

1. Introduction

Drinking water pollution due to agrochemical compounds is the problem for which urgent remedial measures need to be found. As it was shown, among the various semiconductors used in photocatalysis, TiO_2 is essentially the best material for environmental purification. The only drawback of TiO_2 is that its band gap is at 3.2 eV for the anatase and at 3.0 eV for the rutile structure lying in the near-UV region of the electromagnetic spectrum: 385 nm and 410 nm, respectively. As UV light constitutes only 5% of the solar spectrum [1], 95% of the solar photons are unusable for TiO_2 photocatalysis. Therefore, extensive efforts have been made in the development of TiO_2-doped photocatalysts that can utilize solar light more efficiently.

It is generally accepted that the theoretical model of photocatalysis consists of different consecutive steps where each one is essential for the activity and efficiency of the photocatalyst. The initial step of the photocatalytic process consists in the generation of electron-hole pairs upon irradiation of the material with photons whose energies are at least equal to that of the band gap. In this step, parameters like the relation between adsorption/reflection coefficients and the quantum efficiency of electron-hole generation are very important. In the second step, the formed electron-hole pairs can either recombine in the bulk or travel up to the surface, where they can participate in chemical reactions. In this step, the lifetime and the velocity of the electron-hole recombination are of extreme importance. The next step is the creation of H* and OH* radicals as a result of the electron-hole interaction with water, and finally a probable multiple-step reaction of organic compounds with active radicals. In this step, hydrophilic properties of the photocatalytic surfaces are crucial. However so far, the influence of the different stages of this model on the final efficiency of the photocatalysts was not well determined.

Therefore, it is evident that any modification of the TiO_2-based photocatalysts resulting in an improving of the efficiency of the above-described steps will represent a breakthrough in the field. For this purpose, many scientific works have appeared during recent years. A thorough analysis of the different approaches is beyond the scope of this paper,

and only some selected reports will be summarized below. (i) One class of the reports is on the doping of TiO_2 with various transition metals (V, Cr, Mn, Fe, Co, Ni, Au, Ag, Pt, Nb, Cu, W, etc.) to lower the band-gap energy. It was shown by ab initio band calculations based on the density functional theory that an electron-occupied level occurs and electrons are localized around each dopant [2]. As the atomic number of the dopant increases, the localized level shifts to lower energy; thus, for Co the energy level is sufficiently low to be at the top of the valence band, while other metals produce midgap states [2]. In some experimental studies, it was shown that doping with metal ions such as V^{5+}, Cu^{2+}, Fe^{3+}, and W^{6+} leads to an enhanced photoactivity [3, 4] whereas in other studies it was shown to lead to a reduction of the photoactivity [5, 6]. (ii) Another class of reports is on the TiO_2 doping with nonmetals such as N [1, 7–9], S [10–16], F [17], C [8, 18, 19], Br, or Cl [20]. The main idea of nonmetals doping is to create electron-hole trapping centres or charge separating surfaces [21] as well as to shift the optical absorption into the visible region. (iii) A third class of reports is dealing with the increase of the adsorption of pollutants by increasing the hydrophilicity under UV-light illumination [22, 23]. One can suppose that for TiO_2:Fe thin films both of these mechanisms can be activated.

So far, the main obstacle in application of TiO_2 thin films prepared by different techniques is that its photocatalytic activity is much lower than that of the Degussa P25 TiO_2 reference powder. Recently, some new techniques have been developed to prepare pure [24–27] and doped TiO_2 thin films [28–30] to enhance the photocatalytic activities.

Different techniques have been used to prepare doped TiO_2 thin films where Ti or O atoms were partly substituted, namely, pulsed laser deposition ($TiO_{2-x}N_x$ [23]), ion implantation (TiO_2:Fe [28, 31], TiO_2:Sn [29]), cosputtering (TiO_2:Co [30]), deep coating (Fe modified nanotube arrays [32]), or sol-gel methods (TiO_2:Fe [23], TiO_2:Cr [33]).

By the studies of charge separation efficiency, it was recently shown that in the anatase form of TiO_2-oriented thin films, the photo-generated holes can be transported towards the surface once the photon energy irradiation reaches its optical bandgap [34]. By this fact, one can partly explain the enhanced photocatalytic activity of the anatase form in comparison with the rutile form. Recently, a photocatalytic activity of a set of TiO_2 samples with different anatase/rutile ratios, prepared by calcinations at different temperatures from commercial photocatalyst Degussa P25, was studied [35]. Results indicate that samples with higher anatase/rutile ratios presented higher intrinsic activity (intrinsic activity is activity calculated per unit area). Photocatalytic activity was studied for the photodegradation of propane/isobutene/butane (40/35/25%) gas mixture [35]. Photocatalytic activity for aqueous solutions of polluting organic matters of immobilized TiO_2 photocatalysts, such as thin films, can be compared with the activity of Degussa P25 powder (anatase/rutile = 80/20), immobilized on the surface of the substrate.

There are some other important factors that can have strong influence on the photocatalytic activity, namely, the roughness of the photocatalyst surface that determines the active surface, the adhesion of the pollutant molecules to the surface of the photocatalyst, the surface contamination of the photocatalyst, and so on. Therefore, a common standard is needed to compare the photocatalytic activity of TiO_2 photocatalysts prepared by different methods [36].

In this paper, the TiO_2 thin films were prepared using $Ti(dpm)_2(OPr^i)_2$ (dpm = 2,2,6,6-tetramethylheptane-3,5-dione, Pr^i = isopropyl) and $Ti(OPr^i)_4$ (TTIP) as precursors. The volatile compounds $Fe[(C_2H_5)_2NCS_2]_3$ (FeDtc) and $[(CH_3)C]_2S_2$ (di-*tert*-butyldisulphide—TBDS) were used to prepare TiO_2:(Fe, S)-doped films. The P25 Degussa powder was used as standard to compare the photocatalytic activities of the thin films.

2. Methods

2.1. TiO_2 Thin Films Preparation. The TiO_2 films were obtained in a standard vacuum apparatus with a turbomolecular pump (ALCATEL TMP 5400 CP) producing vacuum down to 5×10^{-7} mbar. During the deposition, the pressure of the volatile precursor decomposition products determined the available lower pressure limit. The vaporisation was conducted from an open surface evaporator. The temperature of the vapour source varied in the range of 90°C to 210°C, and the substrate temperature was stabilised around 400°C to 600°C.

Different types of rectangular or round glass and fused silica plates up to 78.5 cm^2 were used as substrates. All substrates were cleaned carefully right before loading using the following procedure. The substrates were cleaned in water using a detergent and then rinsed in distilled water. Afterwards, the substrates were immersed in sulphuric acid (~95%) for about 24 hours, then rinsed by distilled water, washed with acetone, and finally dried by a flux of filtered air.

The film thicknesses, ranging from 30 nm to 2000 nm, were measured by weight. The growth rate was varied from several nanometers to several tens of nanometers per minute.

For the preparation of the doped TiO_2 films, the CVD apparatus was modified by additional gas supply lines allowing to let inert gases (Ar, He) and O_2 into the chamber. The pressure in the CVD chamber was varied between 1.2×10^{-4} mbar and 0.1 mbar, with the system working either in the molecular vapour stream or gas flow regime. The $[(CH_3)C]_2S_2$ (TBDS) was used to dope TiO_2 thin films with sulphur, presumably by substituting some oxygen sites of the TiO_2 crystal structure with sulphur. The TBDS is liquid with a vapour pressure of about 1 mbar at 25°C. The TBDS was placed in an ampoule, heated by a furnace, outside the vacuum chamber, and then connected with the Ar/O_2 gas supply line.

For the preparation of the iron-doped TiO_2 thin films, the $Fe[(C_2H_5)_2NCS_2]_3$ complex compound was used. The temperatures of the evaporating points of TTIP and $Fe[(C_2H_5)_2NCS_2]_3$ are different. Thus, to dope only the surface layers of TiO_2 thin film, a small amount of $Fe[(C_2H_5)_2NCS_2]_3$ was placed into the same evaporator

Table 1: Typical conditions of TiO_2 thin film synthesis.

Sample	Precursor	Substrate	Thickness, nm	T_{sub}, °C	P_{max}, mbar	R, MOhm	Flux, % Ar/O_2^*
1	$Ti(dpm)_2(Opr^i)_2$	Glass	250	540	$1.2 \cdot 10^{-4}$		Vacuum
2		Quartz	250	450	$1.4 \cdot 10^{-4}$		Vacuum
3		Quartz	150	500	$2.4 \cdot 10^{-5}$		Vacuum
4		Quartz	295	550	$1.6 \cdot 10^{-4}$		Vacuum
5		Quartz	300	600	$4.0 \cdot 10^{-4}$		Vacuum
9		Glass	150	450	$1.4 \cdot 10^{-1}$	>200	50/100
10		Glass	215	450	$1.4 \cdot 10^{-1}$	>200	50/100
18		Ceramic	165	465	$1.1 \cdot 10^{-4}$		Vacuum
23	TTIP	Quartz	55	450	$2.1 \cdot 10^{-1}$	>200	100/0
24		Quartz	485	450	$6.4 \cdot 10^{-5}$	>200	Vacuum
26		Glass	250	400	$1.2 \cdot 10^{-4}$		Vacuum
30		Glass	1745	400	$2.1 \cdot 10^{-1}$	>200	50/100
31		Glass	970	450	$3.7 \cdot 10^{-1}$	>200	50/100
65	TTIP + FeDtc (0.008 g)	Glass	970	450	$1.5 \cdot 10^{-1}$	>200	50/100
66	TTIP + TBDS	Glass	970	400	$1.5 \cdot 10^{-1}$		50/100
72	TTIP + FeDtc (0.008 g)	Glass	890	400	$1.1 \cdot 10^{-1}$		50/100
73	TTIP + FeDtc (0.008 g)	Quartz	800	400	$1.1 \cdot 10^{-1}$		50/100
74	TTIP + FeDtc (0.016 g)	Glass	803	400	$1.0 \cdot 10^{-1}$		50/100
75	TTIP + FeDtc (0.016 g)	Quartz	918	400	$1.0 \cdot 10^{-1}$		50/100
76	TTIP + FeDtc (0.032 g)	Glass	516	400	$1.1 \cdot 10^{-1}$		50/100
77	TTIP + FeDtc (0.032 g)	Quartz	593	400	$1.1 \cdot 10^{-1}$		50/100
79	TTIP + FeDtc (0.008 g)	Quartz	1045	400	$1.0 \cdot 10^{-1}$		50/100
80	TTIP + FeDtc (0.016 g)	Glass	560	400	$1.0 \cdot 10^{-1}$		50/100
81	TTIP + FeDtc (0.016 g)	Quartz	580	400	$1.0 \cdot 10^{-1}$		50/100
83	TTIP + FeDtc (0.032 g)	Quartz	760	400	$1.0 \cdot 10^{-1}$		50/100
85	TTIP + FeDtc (0.064 g)	Quartz	480	400	$1.1 \cdot 10^{-1}$		50/100
86	TTIP + FeDtc (0.3 g)	Glass	147	400	$1.1 \cdot 10^{-1}$		50/100
87	TTIP + FeDtc (0.3 g)	Quartz	145	400	$1.1 \cdot 10^{-1}$		50/100

* 100% Flux of Ar and oxygen correspond to 20 mL/min at normal pressure.

used for the TTIP evaporation. These two complex compounds were separated in order to avoid a chemical interaction. To prepare uniformly doped TiO_2 thin films, the $Fe[(C_2H_5)_2NCS_2]_3$ was placed into the evaporator inside the vacuum chamber and the TTIP into the evaporator outside the vacuum chamber. The vapours of TTIP were admitted into the vacuum chamber by an Ar/O_2 flux. By the use of $Fe[(C_2H_5)_2NCS_2]_3$, some Ti sites in the TiO_2 crystal structure are presumably substituted by Fe. However, since each molecule of $Fe[(C_2H_5)_2NCS_2]_3$ contains Fe–S bonds, this substitution may be complex which could mean, that not only Ti sites will be substituted by Fe atoms, but also that oxygen sites are being substituted by sulphur. As shown, the FeS_x films resulting from the decomposition of $Fe[(C_2H_5)_2NCS_2]_3$ in vacuum can be easily transformed into FeO_x films depending on the oxygen pressure [37]. So, the concentration of sulphur can be tuned by the changes in the Ar/O_2 ratio independently of Fe concentration. Some of the film preparation conditions are summarised in Table 1.

2.2. Characterization Methods. Structural information on as-prepared TiO_2 thin films was obtained from synchrotron radiation experiments. High-resolution grazing-incidence X-ray diffraction (GIXRD) as well as θ-2θ experiments were performed at the high-resolution powder diffractometer at the DESY/HASYLAB synchrotron radiation laboratory, using synchrotron radiation wavelength equal to λ = 0.0709494 nm. Thin films deposited on either glass or fused silica substrates were analysed.

The trace analysis of the TiO_2 films was performed by laser ionization mass spectrometry (LIMS). A double-focusing mass spectrometer with Mattauch-Herzog geometry and laser plasma ion source (EMAL-2) was used. The energy output of Nd-YAG laser (wavelength of 1064 nm); pulse duration; repetition rate; diameter of laser spot on sample surface were adjusted to evaporate and ionize of the deposited films only. The glass substrates are transparent for Nd-YAG laser radiation and were not destroyed. At the chosen radiation power density ($\sim 1 \times 10^9$ W/cm^2), the measured concentration of Si (main component of the substrate) was not exceeding 10^{-2}% wt. Step motors provided the scanning of the samples in two directions (X-Y). The area of the analyzed surface was about 0.5 cm^2. The concentrations of the impurities were evaluated with respect to the Ti (matrix element of deposited layer) as the internal standard.

Scanning electron microscopy (SEM) was used to perform surface imaging and bulk compositional analysis of doped TiO_2:(Fe, S) samples. The Zeiss Supra 25 field emission SEM (FESEM) microscope with currently highest resolution (~2 nm), equipped with a liquid nitrogen-free, Peltier cooled (cooling time < 30 s) EDX detector X-Flash 3001 with Quantax (Bruker AXS, Berlin, Germany) was used.

The TiO_2 films were analysed by X-ray photoelectron spectroscopy (XPS) using XSAM800 (KRATOS) X-ray spectrometer operated in the fixed analyser transmission (FAT) mode. A Mg K_α (1253.7 eV) X-ray source was used. The analyser was operated at 20 eV pass energy both for detail and survey spectra. All the binding energies were referenced to the C 1s peak at 285.0 eV or O 1s peak at 529.9 eV.

Atomic force microscopy measurements were performed on a Solver PRO Scanning Probe Microscope at room temperature and atmospheric pressure in a contact mode with feedback control switched on.

The transmission coefficient of the TiO_2 films prepared on the quartz substrates was measured using a "Cintra-40" UV-Vis spectrophotometer. The absorbance onset at 390 nm corresponds to the TiO_2 semiconductor gap width.

Conversion electron Mössbauer spectroscopy (CEMS) was performed at roomtemperature on a Wissel constant acceleration spectrometer, using a Rikon-5 detector and a 57Co/Rh source. The resulting spectra were calibrated with alpha-Fe foil and fitted using an integrated least-squares computer program to determine the hyperfine parameters.

The layout of the photoreactor apparatus is described in detail in [38]. Briefly, the volume of irradiated solution was of 7.9 mL at 1 mm optical thickness. A 200 W Xenon lamp was used as a UV light source, and a water filter with fused silica windows was used in order to avoid an excessive heating of the solution. The photocatalytic process in water requires the presence of O_2 as electron acceptor; thus, a continuous flow of air was injected by means of an air pump. Fenarimol (Riedel, 99.7%) 5 mg/L solutions were prepared in bidistilled water. The Fenarimol solution was left in contact with the reactor cell about 12 h in the dark before irradiation in order to achieve the adsorption equilibrium of the pesticide between the solution and the cell surfaces. During irradiation, 100 μL samples were taken every 0.5 h or 1 h and immediately analysed on an HPLC system (Merck-Hitachi 655A-11 system with 655A-22 UV detector) under the following experimental conditions: LichroCART 125-4 column: Lichrospher 100 RP-18, 5 μm; eluent: acetonitrile (Merck Lichrosolv) 65%, bidistilled water 35%; 1,1 mL/min flow; UV detection at 220 nm. The total irradiation time was between 3 and 5 hours for each sample. To compare the reaction rates obtained for the thin films, commercial TiO_2 P25 powder (Degussa) with identical amount by weight (7 mg) was deposited on fused silica substrates by evaporation from a TiO_2 aqueous suspension and tested under identical experimental conditions as the CVD films.

3. Results and Discussion

XRD studies of crystal structure for samples prepared with the precursor $Ti(dpm)_2(OPr^i)_2$ as well as thermal decomposition mass spectrometry studies for the precursor $Ti(dpm)_2(OPr^i)_2$ in vacuum and in the presence of oxygen were reported in detail earlier [38, 39]. In the present work, thin films prepared from precursors $Ti(dpm)_2(OPr^i)_2$, TTIP, and doped TiO_2:(Fe, S) were studied using θ-2θ configuration of XRD. The most significant difference between films deposited from precursors $Ti(dpm)_2(OPr^c)_2$ and TTIP is that for precursor $Ti(dpm)_2(OPr^i)_2$, polycrystalline rutile films were obtained, while for TTIP the films consist of polycrystalline anatase. It is important to emphasize that the synthesis conditions for films derived from both precursors were very similar (see Table 1), and the resulting crystal structure was independent of the substrate (glass, fused silica or Si-wafer). Thus, the choice of the precursor can be used to control the form of the titanium dioxide produced. It was noted that there is a difference in the thin film crystal orientation, when TiO_2 films have been prepared with TTIP precursor placed into the evaporator inside or outside the vacuum chamber. We suppose that the difference in the microcrystal orientation is due to differences in the vapour content of the TTIP precursor evaporated at different conditions. According to the XRD results, the presence of Fe and S in the crystal structure of TiO_2 thin films does not change the type of crystal modification, and it remains the anatase structure. Typical XRD patterns are shown in Figures 1 and 2. No additional peaks belonging to separate iron oxides are observed.

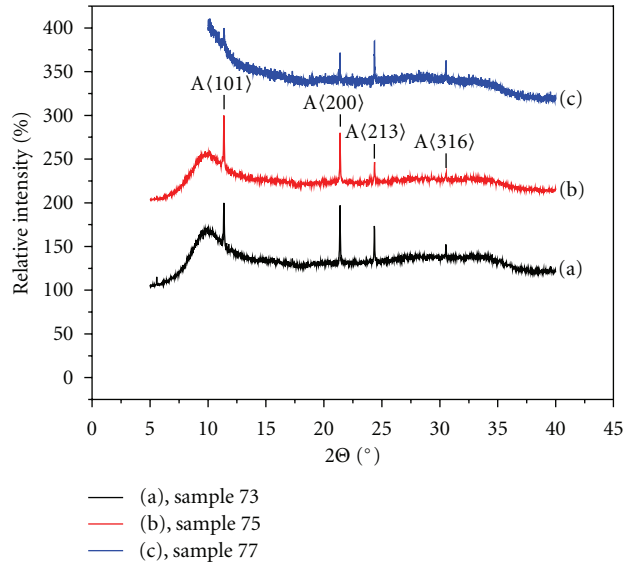

Figure 1: X-ray diffraction patterns for anatase TiO_2:(Fe, S) thin films obtained from the internal evaporator in a controlled Ar/O_2 atmosphere.

Average concentration of impurities in the TiO_2 films was obtained by laser ionization mass spectrometry. The results of the LIMS analysis are shown at Table 2.

All the analyzed samples were synthesized on fused silica substrates, so that the presence of Na and Ca is relatively small and the presence of these elements should be related to the heated parts used in the construction of the substrate heater. Large sample to sample contamination variability

Table 2: The results of mass-spectrometry analysis; the values are shown in %. n/d: not detected; the detectability threshold is given in brackets.

Impurity	Sample 1	Sample 2	Sample 3	Sample 4	Sample 5
C	$\approx 5 \cdot 10^{-1}$	$\approx 5 \cdot 10^{-1}$	$\approx 5 \cdot 10^{-1}$	$\approx 5 \cdot 10^{-1}$	$\approx 5 \cdot 10^{-1}$
N	$\leq 2 \cdot 10^{-2}$	$\leq 2 \cdot 10^{-2}$	$\leq 2 \cdot 10^{-2}$	$\leq 4 \cdot 10^{-2}$	$\leq 4 \cdot 10^{-2}$
Na	$< 2 \cdot 10^{-1}$	$< 2 \cdot 10^{-1}$	$< 2 \cdot 10^{-1}$	$< 2 \cdot 10^{-1}$	$< 2 \cdot 10^{-1}$
Mg	$< 1 \cdot 10^{-2}$	$< 1 \cdot 10^{-2}$	$< 1 \cdot 10^{-2}$	$< 1 \cdot 10^{-2}$	$< 1 \cdot 10^{-2}$
Al	$5 \cdot 10^{-3}$	$3 \cdot 10^{-2}$	$7 \cdot 10^{-3}$	$4 \cdot 10^{-3}$	$1 \cdot 10^{-2}$
P	$3 \cdot 10^{-3}$	$3 \cdot 10^{-3}$	$3 \cdot 10^{-3}$	$1 \cdot 10^{-3}$	$2 \cdot 10^{-3}$
Cl	$1 \cdot 10^{-2}$	$5 \cdot 10^{-2}$	$1 \cdot 10^{-2}$	$7 \cdot 10^{-3}$	$4 \cdot 10^{-2}$
K	$2 \cdot 10^{-1}$	$4 \cdot 10^{-2}$	$2 \cdot 10^{-2}$	$1 \cdot 10^{-2}$	$2 \cdot 10^{-2}$
Ca	$7 \cdot 10^{-2}$	$1 \cdot 10^{-1}$	$3 \cdot 10^{-2}$	$8 \cdot 10^{-2}$	$8 \cdot 10^{-2}$
Cr	$1 \cdot 10^{-3}$	$7 \cdot 10^{-4}$	$5 \cdot 10^{-4}$	$1 \cdot 10^{-3}$	$5 \cdot 10^{-3}$
Mn	$6 \cdot 10^{-4}$	$1 \cdot 10^{-3}$	$9 \cdot 10^{-4}$	$3 \cdot 10^{-4}$	$1 \cdot 10^{-3}$
Fe	$1 \cdot 10^{-2}$	$3 \cdot 10^{-1}$	$2 \cdot 10^{-1}$	$1 \cdot 10^{-1}$	$1 \cdot 10^{-1}$
Co	n/d ($6 \cdot 10^{-4}$)	n/d ($6 \cdot 10^{-4}$)	n/d ($6 \cdot 10^{-4}$)	n/d ($6 \cdot 10^{-4}$)	n/d ($6 \cdot 10^{-4}$)
Ni	$2 \cdot 10^{-3}$	$8 \cdot 10^{-4}$	n/d ($6 \cdot 10^{-4}$)	n/d ($6 \cdot 10^{-4}$)	$5 \cdot 10^{-3}$
Cu	$3 \cdot 10^{-3}$	$4 \cdot 10^{-1}$	$2 \cdot 10^{-1}$	$1 \cdot 10^{-1}$	$1 \cdot 10^{-1}$
Zn	$3 \cdot 10^{-2}$	$4 \cdot 10^{-2}$	$1 \cdot 10^{-1}$	$2 \cdot 10^{-2}$	$5 \cdot 10^{-2}$

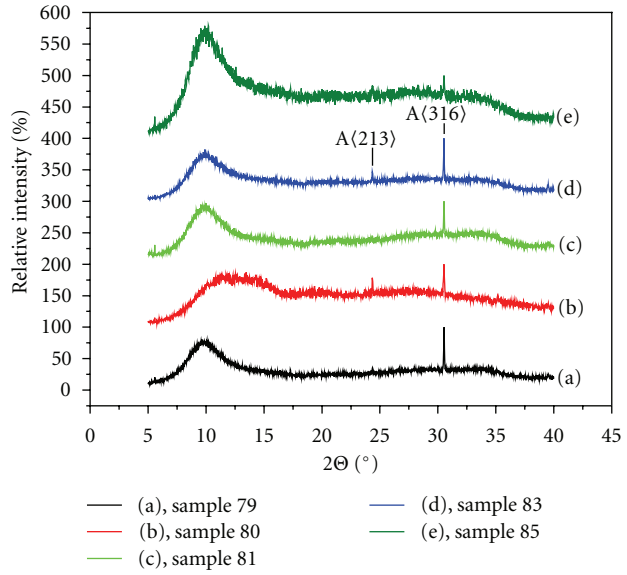

Figure 2: X-ray diffraction patterns for anatase TiO_2:(Fe, S) thin films obtained from the external evaporator in a controlled Ar/O_2 atmosphere.

is observed for Fe, Cu, K, and Zn. The origin of the Zn contamination for sample 3 and the K contamination for sample 1 is not yet clear. The Fe and Cu impurities probably originate from the interaction of the precursor vapors with the metallic parts of the CVD apparatus. The presence of C at $5 \cdot 10^{-1}$% wt can be attributed to the residual carbon deposited during the process of the precursor decomposition.

Some typical images of the surfaces of TiO_2:(Fe, S) samples obtained by SEM are shown in Figures 3(a) and 3(b). Elemental analysis obtained by EDX (e.g., sample 72) is shown in Figure 4 and Table 3. EDX spectra were taken at the sample angles of 30° and 60° to examine influence of the substrate. Analysis shows that there are not significant differences in the spectra between these both positions of the sample.

XPS spectra were taken at the angle of 0° and 60° relative to the normal to the surface of the sample in order to document the changes in composition of the film in dependence of the depth near the surface. The relative contents of the elements are given in Table 4. The XPS results demonstrated that samples 30 and 31 are slightly contaminated with sodium and zinc, respectively. The origin of this contamination is unclear. These samples were analysed by XPS after their photocatalytic activity studies were performed. Therefore, these contaminations may originate from the aqueous solutions that have been in contact with the sample surface. Comparing the mass spectrometry data with those of the XPS analysis, we note that a larger concentration of carbon is found on the surface compared to the bulk, indicating the redistribution of carbon during thin-film growth. Several process parameters affect the surface contamination by carbon, including the synthesis temperature, the oxygen concentration in the vapour phase during film growth, and the type of precursor.

The total carbon content decreases with increasing process temperature for samples synthesized from $Ti(dpm)_2(OPr^i)_2$ in vacuum. The carbon content is also lower for samples prepared in the presence of oxygen under otherwise identical conditions, which may be explained in at least two different ways. Firstly, as it was shown by mass spectrometric analysis of the $Ti(dpm)_2(OPr^i)_2$ decomposition products that the thermolysis mechanism is different in vacuum and in presence of oxygen [39].

Secondly, the decomposition products will form gaseous CO and CO_2 much more easily in the presence of oxygen than in vacuum. The total carbon content of the samples prepared from TTIP in the presence of oxygen is even lower

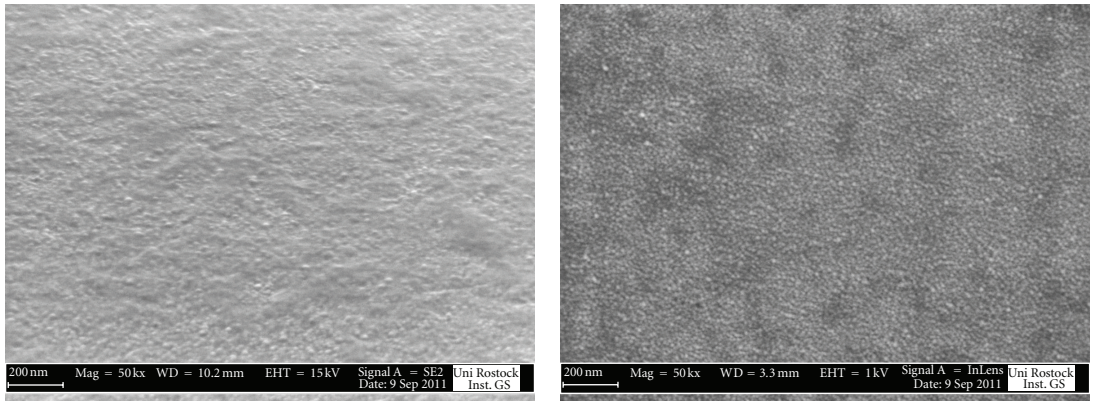

(a) (b)

Figure 3: (a) SEM image of the TiO_2:(Fe, S) sample 72. (b) SEM image of the TiO_2:(Fe, S) sample 74.

Table 3: Quantitative results of the EDX analysis of TiO_2:(Fe, S), sample 72.

Element	OZ	Series	Netto	C, wt% normalized	C, at%
C	6	K-series	3957	0.96	1.60
Na	11	K-series	79956	9.62	8.43
Mg	12	K-series	23091	2.42	2.01
Al	13	K-series	7444	0.73	0.55
Si	14	K-series	285189	28.55	20.47
S	16	K-series	922	0.11	0.07
K	19	K-series	3966	0.66	0.34
Ca	20	K-series	20759	4.29	2.15
Ti	22	K-series	6252	1.94	0.82
Fe	26	K-series	457	0.29	0.10
O	8	K-series	201328	50.43	63.46

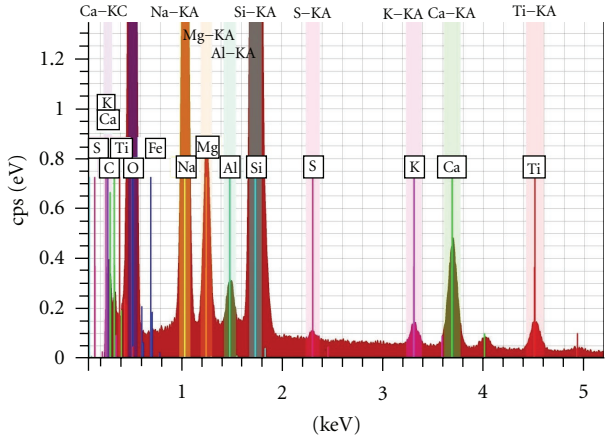

Figure 4: EDX spectrum of the TiO_2:(Fe, S), Sample 72.

and increases with increasing processing temperature, which is probably related to a different kinetic mechanism of thin-film growth. The latter hypothesis is supported by the fact that the crystal structures of the films prepared from the two precursors are different.

Comparing the results of LIMS, EDX, and XPS tests, Tables 2, 3, and 4, it can be concluded that the initial presence of Fe, without doping, is at a concentration of about 0.1%, and S is not found by LIMS. When a small amount of the precursor FeDtc (of 0.008 g and 0.016 g) had evaporated, a small concentration of Fe and S was detected by EDX in the volume of the films. However, as the analysis of XPS Fe and S does not register them in the surface layers, this means that the concentration of Fe and S in these layers is less than the detection limit by the XPS (around 0.1%).

The surface morphology of the TiO_2:Fe thin films was investigated as a function of various parameters, such as thickness, the type of substrate, percentage of doping element, and the mode of deposition, meaning deposition from the interior or exterior sources of the precursor vapours. The AFM results demonstrated that the TiO_2 film samples have a porous polycrystalline structure with a typical crystallite size of about 100 nm. The results of the AFM studies are shown in Figures 5(a)–5(d) and 6(a)–6(d) and in Table 5. As it can be seen, the surface roughness does not depend on the type of substrate (Figures 5(a) and 5(b)). However, the surface roughness depends on the thin film thickness, the mode of the film preparation, and on the doping element concentration. Average crystallite size data was determined from AFM

Table 4: Composition (atom percentage, %) of TiO_2 films according to XPS analyses (The composition is shown for XPS spectra taken at 0°).

Attribution		Sample 1	Sample 30	Sample 31	Sample 65	Sample 66	Sample 75	Sample 77	Sample 85
Ti, 2p	Ti	12.9	20.9	20.7	21.7	22.0	18.34	16.93	11.2
Oxygen, 1s	O	40.7	63.2	59.0	61.24	59.4	52.72	51.84	43.65
Carbon total	C	39.0	14.8	20.3	17.1	22.0	23.21	27.1	33.0
Fluorine, 1s	F	—	—	—	—	—	5.2	2.34	8.04
Sodium, 1s	Na	—	—	—	—	—	—	—	3.0
Iron, 2p	Fe	—	—	—	—	—	—	1.02	0.47
Sulphur, 2p	S	—	—	—	—	—	0.53	0.77	0.57
Stoichiometry		TiO2.4	TiO2.48	TiO2.47	TiO2.25	TiO2.25	TiO2.22	TiO2.3	TiO2.2

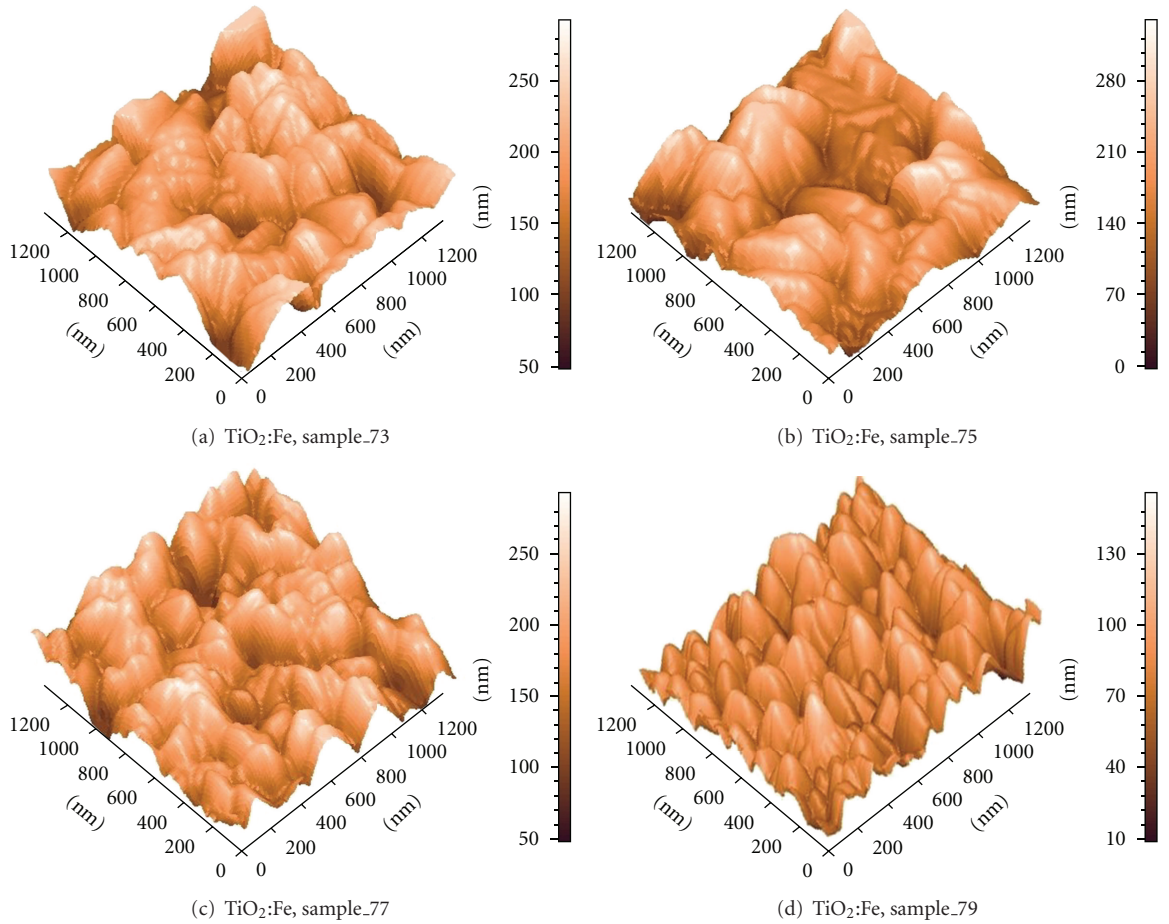

(a) TiO_2:Fe, sample_73

(b) TiO_2:Fe, sample_75

(c) TiO_2:Fe, sample_77

(d) TiO_2:Fe, sample_79

Figure 5: The AFM image of the samples with the thin film thickness 600–1000 nm (the field size is 1.2 μm by 1.2 μm; the shades of grey correspond to the vertical scale of the recording of 0 to 250 nm). Samples 73–77 (internal evaporator), sample 79, (external evaporator).

analysis. This analysis was found to give data whose values are coincident with those obtained by X-ray line broadening using Warren-Averbach analysis [40]. The average crystallite sizes in dependence on the thin films thicknesses are shown in Figure 7. It is important to note that when the concentration of Fe was increased, the average crystallite size was found to be decreased. It can be noted that the usage of the internal evaporator also leads to much bigger crystallite sizes.

Figure 8 shows the UV-Vis transmittance spectra of the prepared samples. The absorption threshold of all the samples TiO_2:Fe (1–5%) is about 370 nm to −385 nm, which corresponds to the band-gap energy of anatase (3.2 eV). The film thickness of the samples 73 and 75 is about 1 μm; therefore, the transmittance in the visible range of the light spectrum is not high (about 50%), and it is not connected with the photon adsorption due to the presence of the Fe impurities. The transmittance spectra of the heavy doped Sample 87 is different because of the mixing of TiO_2 and Fe_3O_4 phases. With the increasing content of Fe, the prepared samples acquired a reddish tinge, while sample 87 turned pale red.

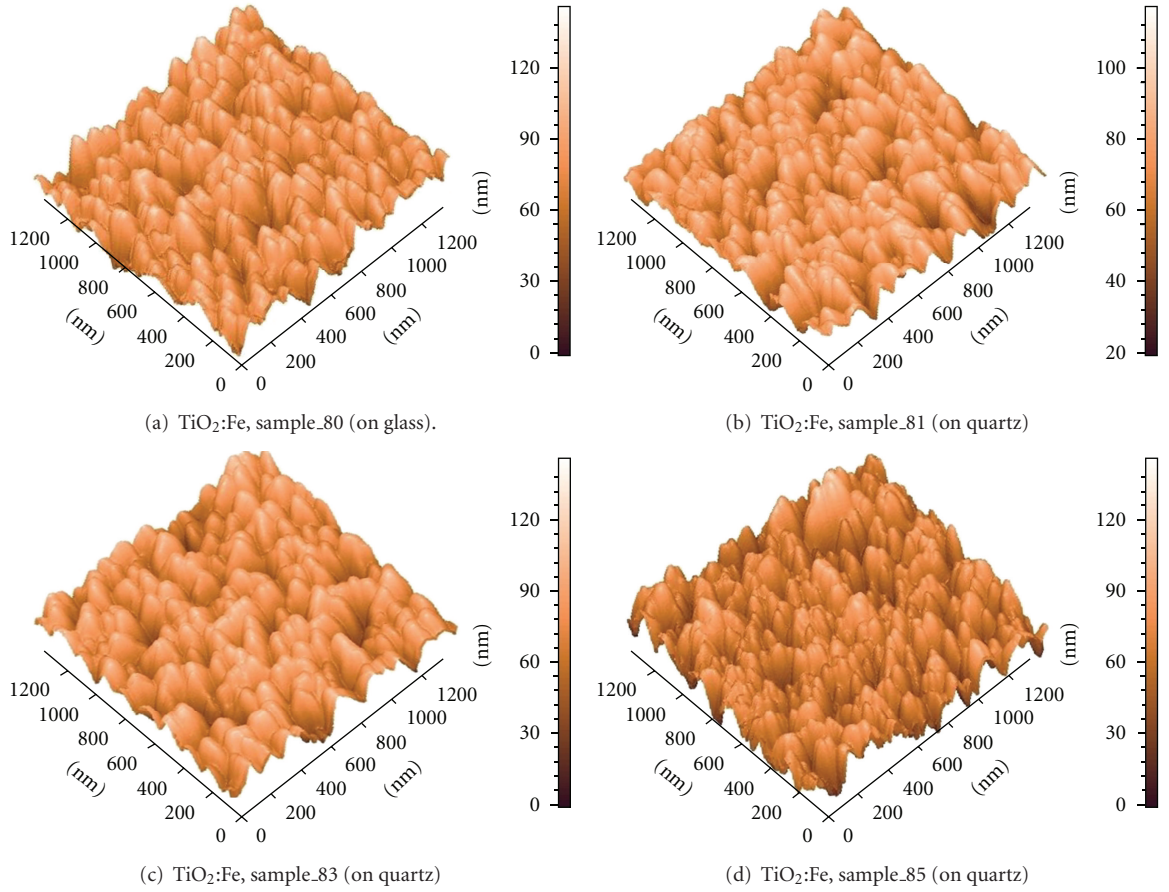

(a) TiO_2:Fe, sample_80 (on glass).

(b) TiO_2:Fe, sample_81 (on quartz)

(c) TiO_2:Fe, sample_83 (on quartz)

(d) TiO_2:Fe, sample_85 (on quartz)

Figure 6: The AFM image of the sample with the thin film thickness ~500 nm (the field size is 1.2 μm by 1.2 μm; the shades of grey correspond to the vertical scale of the recording of 0 to 250 nm). External evaporator.

Table 5: Surface morphology data of the samples TiO_2:Fe obtained by AFM.

Sample	Film thickness (nm)	Quantity of FeDtc in the evaporator (g)	Evaporation mode	Maximum size, h (nm)	Medium size $\langle h \rangle$ (nm)	Medium irregularity $S_{\Delta h}$ (nm)
73	800	0.008	Internal	381	203	51.8
75	918	0.016	Internal	370	208	51.2
77	593	0.032	Internal	338	228	36.1
79	1045	0.008	External	215	104	22.8
80	560	0.016	External	142	72	13.3
81	580	0.016	External	134	84	15.1
83	760	0.032	External	183	114	18.2
85	480	0.064	External	120	67	11.8
87	145	0.300	External	79	39	10.1

The conversion electron Mössbauer spectra (CEMS) recorded from sample 87 are shown in Figure 9. It consists of a single sextet, which suggests magnetic ordering of the Fe^{3+} ions. As shown recently [41], at ^{57}Fe concentrations of about 0.1% to −1%, CEMS spectra exhibit the doublet lines of the hyperfine splitting. The effects of magnetic correlations were explained by the existence of the bound magnetic polaron (BMP) mechanism [41]. CEMS spectra obtained in this study were obtained for the samples with the concentration of Fe that is much higher, because of a small concentration of isotope ^{57}Fe in FeDtc precursor. The ordering type of magnetite (Fe_3O_4) was observed.

The kinetics of the Fenarimol decay and the kinetics of its intermediate photoproduct (m/z 328) formation for different thin films are shown in Figures 10(a) and 10(b), respectively. Abundances of Fenarimol and the intermediate photoproduct are expressed here by the respective chromatographic peak areas, which for the same experimental conditions are

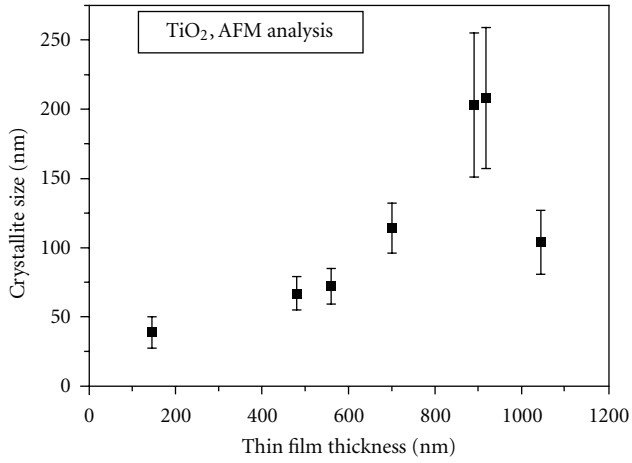

Figure 7: Results of AFM analysis of average particle sizes in anatase TiO_2 thin films in dependence on thin film thickness.

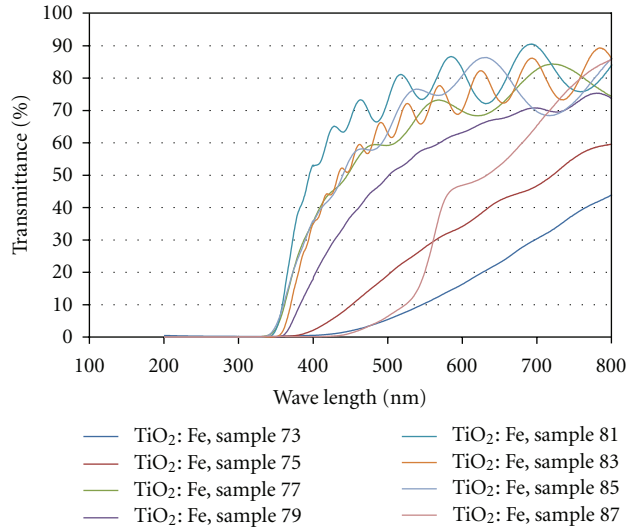

Figure 8: Transmittance UV-Vis spectra of iron doped TiO_2 thin films. Samples 73–77 were prepared from the internal, and Samples 79–87 from the external precursors vapor source.

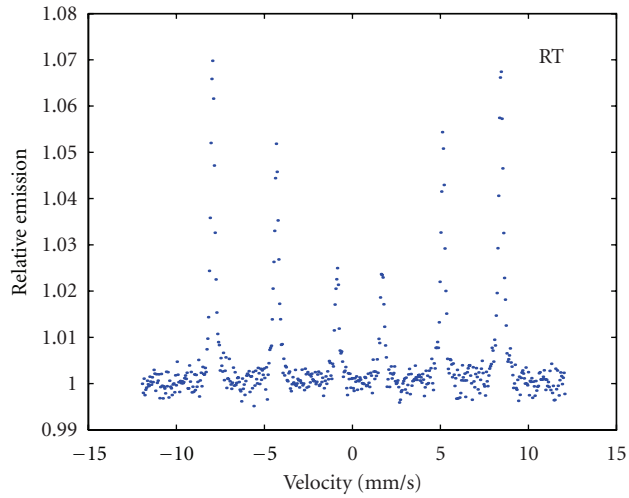

Figure 9: Mössbauer spectra of the TiO_2:Fe, Sample 87 at room temperature (RT).

proportional to the chemical concentration for each instant of analysis time.

Of all the films tested, the TiO_2 films prepared from TTIP were the only samples to exhibit photocatalytic activity. As one can see, only for these samples the concentration of intermediate photoproducts starts to decrease after about 1.5 hours of irradiation. The photocatalytic performance of the same weight of the Degussa P25 powder deposited on glass is still better than that of the CVD films (Figure 10). However, one should take the difference in the specific area of the CVD thin films and that of the Degussa powder film into account. The CVD films grown for this study had a good transparency to the eye. AFM images revealed the film crystallites of about 100 nm in diameter. Therefore, following [24], we may presume the electrode-specific surface area was not very different from the geometric area (~0.00785 m^2). In the case where 7 mg, the typical mass of a CVD film, of the Degussa P25 powder was dissolved in water, the specific area would be about 0.35 m^2 supposing well-separated microcrystals (about 50 m^2/g [22]). However, it is clear that powder deposited on the glass substrate does not have such a big specific surface area. As follows from Figure 10(a), samples 65 and 66 were the most active photocatalytic thin films. Samples 65 and 66 were prepared from TTIP + FeDtc (0.008 g) and 66 from TTIP + TBDS (Vapours), respectively (see Table 1), so that the first sample is supposed to be doped with Fe and with S, and the second sample only with S. However, the XPS analysis did not show the presence of Fe or S on the surface layer of these samples. The relative concentration of other elements (Ti, O, and C) revealed by XPS is typical for the samples prepared from TTIP (see Table 4). Further increase of the amount of FeDtc precursor during the synthesis (samples 75, 77 and 85) resulted in the preparation of the TiO_2:(Fe, S)-doped thin films as it was shown by XPS. However, the photocatalytic activity of these samples is lower than that of 65 and 66 samples. It was also found that samples 75, 77, and 85 are contaminated with fluorine, the source of such contamination and its influence on photocatalytic activity is not established yet.

After analysis of the obtained results, the following can be stated: (1) the TiO_2:(Fe, S) thin films, prepared from TTIP by CVD, are in the anatase form, which is most effective for photocatalysis. (2) The most effective surface was observed for the films with the thickness of about 1 μm. Just this kind of films was used in the studies of photocatalytic efficiency. (3) There is no presence of crystalline iron oxide phases in TiO_2:(Fe, S) thin films revealed by XRD. (4) When the concentration of Fe is low, the transmittance spectra are similar to those of nondoped thin films. For this reason, the UV part of the radiation spectrum was used to compare the photocatalytic activity of TiO_2:(Fe, S) thin films with that of Degussa P25 powder. (5) According to theoretical results, the doping of TiO_2 with transitional metals, such as Fe, leads to the appearance of electronic states inside the band-gap of TiO_2 and, thus, to an increase of the photocatalytic efficiency.

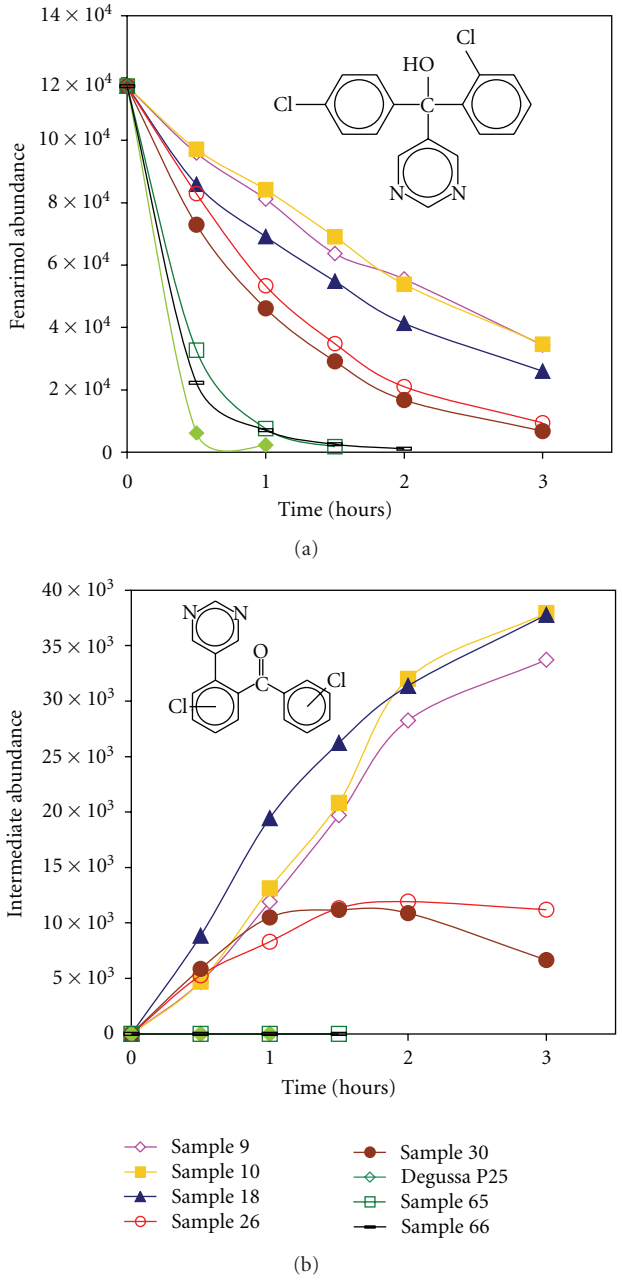

FIGURE 10: Contents of Fenarimol solution (a) and intermediate photoproduct (b) in dependence on time, under UV illumination, when in contact with several different TiO_2 thin films.

Therefore, the increased photocatalytic activity of optimally prepared TiO_2:(Fe, S) thin films in the UV region can be expected in comparison with non-doped Degussa P25 powder. It can be seen, that in the experiments on Fenarimol photocatalytic decay, the photocatalytic activity (PhAc) of TiO_2:(Fe, S) (PhAc(TiO:Fe)) is comparable with that of Degussa P25 (PhAc(P25)), but PhAc(TiO:Fe) is still lower than PhAc(P25).

There is a contradiction with the theoretical model. It can be pointed out that the hydrophilicity of TiO_2:Fe is anomalously high under UV light irradiation [24, 25]. This means the presence of anchoring water splitting centres and, as a result, the more effective creation of H^+ and OH^- radicals. This effect is supposed to be favourable for PhAc(TiO:Fe). In practice, this does not lead to greater PhAc(TiO:Fe) in the UV region as compared to PhAc(P25). It can be assumed that the generation of electron-hole pairs at the Fe impurity gives a small contribution to the PhAc(TiO:Fe). It was shown earlier (see, e.g., [42]) that PhAc(doped TiO_2) is higher than PhAc(non-doped TiO_2 and P25) in the visible light region. In the UV region the PhAc(doped TiO_2) is still lower than the PhAc(P25). This only means that the excitation mechanisms of electron-hole pair through the TiO_2 bandgap by incident photons with energy lower than band-gap energy is switched off in the main mechanism of photocatalysis. Powder P25 also has some PhAc(P25) in visible light region, possibly due to lattice defects and impurities.

4. Conclusions

The physical and photocatalytic properties of thin films TiO_2:Fe and TiO_2:S prepared by CVD using complex compound precursors, $Ti(dpm)_2(OPr^i)_2$, $Ti(OPr^i)_4$, and $Fe[(C_2H_5)_2NCS_2]_3$, $[(CH_3)C]_2S_2$(TBDS) were discussed. Two different crystalline forms, rutile and anatase, could be prepared using these precursors, as demonstrated by XRD. LIMS and XPS analysis revealed that the surface composition is different from that of the film, basically because of carbon presence. From the results of LIMS, EDX, and XPS tests for low-doped samples, it can be concluded that small concentrations of Fe and S of both elements are present in the films. As it is shown from the Mössbauer spectra, Fe ions are magnetically ordered in the heavy-doped TiO_2 thin films. By this fact, the lowering of the photocatalytic activity due to existence of the additional channel of the photon energy relaxation can be explained. The structure of TiO_2 thin film photocatalyst has a dominating effect on the photodegradation rate of the Fenarimol test compound, namely only the anatase form of pure and doped TiO_2 thin films shows photocatalytic activity. It was shown that an increased photocatalytic activity of (Fe, S)-doped TiO_2 thin-films is, actually, very close to Degussa P25 powder activity. However, to answer the question of what exactly happened with this kind of substitution of Ti or O sites by Fe and S in TiO_2, further studies by XPS and nuclear resonant methods using synchrotron radiation are needed.

Acknowledgments

The authors are grateful to Fundação para a Ciência e Tecnologia for the financial support given in the framework of the Projects POCTI/43520/FIS/2000 and CONC-REEQ/700/2001. The steady support of HASYLAB is highly appreciated. The authors thank R. Lange for the technical assistance with SEM and EDX. The collaboration with M. Stir and R. C. Nicula in the initial phase of this work is gratefully acknowledged.

References

[1] S. Yin, Q. Zhang, F. Saito, and T. Sato, "Preparation of visible light-activated titania photocatalyst by mechanochemical method," *Chemistry Letters*, vol. 32, no. 4, pp. 358–359, 2003.

[2] T. Umebayashi, T. Yamaki, H. Itoh, and K. Asai, "Analysis of electronic structures of 3d transition metal-doped TiO_2 based on band calculations," *Journal of Physics and Chemistry of Solids*, vol. 63, no. 10, pp. 1909–1920, 2002.

[3] J. Zhu, W. Zheng, B. He, J. Zhang, and M. Anpo, "Characterization of Fe-TiO_2 photocatalysts synthesized by hydrothermal method and their photocatalytic reactivity for photodegradation of XRG dye diluted in water," *Journal of Molecular Catalysis A*, vol. 216, no. 1, pp. 35–43, 2004.

[4] A. Di Paola, G. Marcì, L. Palmisano et al., "Preparation of polycrystalline TiO_2 photocatalysts impregnated with various transition metal ions: characterization and photocatalytic activity for the degradation of 4-nitrophenol," *Journal of Physical Chemistry B*, vol. 106, no. 3, pp. 637–645, 2002.

[5] D. W. Bahnemann, S. N. Kholuiskaya, R. Dillert, A. I. Kulak, and A. I. Kokorin, "Photodestruction of dichloroacetic acid catalyzed by nano-sized TiO_2 particles," *Applied Catalysis B*, vol. 36, no. 2, pp. 161–169, 2002.

[6] K. Nagaveni, M. S. Hegde, and G. Madras, "Structure and photocatalytic activity of $Ti_{1-x}M_xO_{2\pm\delta}$ (M = W, V, Ce, Zr, Fe, and Cu) synthesized by solution combustion method," *Journal of Physical Chemistry B*, vol. 108, no. 52, pp. 20204–20212, 2004.

[7] R. Asahi, T. Morikawa, T. Ohwaki, K. Aoki, and Y. Taga, "Visible-light photocatalysis in nitrogen-doped titanium oxides," *Science*, vol. 293, no. 5528, pp. 269–271, 2001.

[8] I. N. Martyanov, S. Uma, S. Rodrigues, and K. J. Klabunde, "Structural defects cause TiO_2-based photocatalysts to be active in visible light," *Chemical Communications*, vol. 10, no. 21, pp. 2476–2477, 2004.

[9] G. Shang, H. Fu, S. Yang, and T. Xu, "Mechanistic study of visible-light-induced photodegradation of 4-chlorophenol by TiO_{2-x} N_x $0.021 < x < 0.049$ with low nitrogen concentration," *International Journal of Photoenergy*, vol. 2012, Article ID 759306, 2012.

[10] T. Umebayashi, T. Yamaki, H. Itoh, and K. Asai, "Band gap narrowing of titanium dioxide by sulfur doping," *Applied Physics Letters*, vol. 81, no. 3, p. 454, 2002.

[11] T. Ma, M. Akiyama, E. Abe, and I. Imai, "High-efficiency dye-sensitized solar cell based on a nitrogen-doped nanostructured titania electrode," *Nano Letters*, vol. 5, no. 12, pp. 2543–2547, 2005.

[12] C. Di Valentin, G. Pacchioni, A. Selloni, S. Livraghi, and E. Giamello, "Characterization of paramagnetic species in N-doped TiO_2 powders by EPR spectroscopy and DFT calculations," *Journal of Physical Chemistry B*, vol. 109, no. 23, pp. 11414–11419, 2005.

[13] S. Livraghi, A. Votta, M. C. Paganini, and E. Giamello, "The nature of paramagnetic species in nitrogen doped TiO_2 active in visible light photocatalysis," *Chemical Communications*, no. 4, pp. 498–500, 2005.

[14] S. Livraghi, M. C. Paganini, E. Giamello, A. Selloni, C. Di Valentin, and G. Pacchioni, "Origin of photoactivity of nitrogen-doped titanium dioxide under visible light," *Journal of the American Chemical Society*, vol. 128, no. 49, pp. 15666–15671, 2006.

[15] A. Ghicov, J. M. Macak, H. Tsuchiya et al., "Ion implantation and annealing for an efficient N-doping of TiO_2 nanotubes," *Nano Letters*, vol. 6, no. 5, pp. 1080–1082, 2006.

[16] M. Batzill, E. H. Morales, and U. Diebold, "Influence of nitrogen doping on the defect formation and surface properties of TiO_2 rutile and anatase," *Physical Review Letters*, vol. 96, no. 2, Article ID 026103, 2006.

[17] T. Yamaki, T. Umebayashi, T. Sumita et al., "Fluorine-doping in titanium dioxide by ion implantation technique," *Nuclear Instruments and Methods in Physics Research B*, vol. 206, pp. 254–258, 2003.

[18] Y. Choi, T. Umebayashi, S. Yamamoto, and S. Tanaka, "Fabrication of TiO_2 photocatalysts by oxidative annealing of TiC," *Journal of Materials Science Letters*, vol. 22, no. 17, pp. 1209–1211, 2003.

[19] X. Hong, Z. Wang, W. Cai et al., "Visible-light-activated nanoparticle photocatalyst of iodine-doped titanium dioxide," *Chemistry of Materials*, vol. 17, no. 6, pp. 1548–1552, 2005.

[20] H. Luo, T. Takata, Y. Lee, J. Zhao, K. Domen, and Y. Yan, "Photocatalytic activity enhancing for titanium dioxide by co-doping with bromine and chlorine," *Chemistry of Materials*, vol. 16, no. 5, pp. 846–849, 2004.

[21] L. Zhao, J. Ran, Z. Shu, G. Dai, P. Zhai, and S. Wang, "Effects of calcination temperatures on photocatalytic activity of ordered titanate nanoribbon/SnO_2 films fabricated during an EPD process," *International Journal of Photoenergy*, vol. 2012, Article ID 472958, 2012.

[22] A. Mills, N. Elliott, I. P. Parkin, S. A. O'Neill, and R. J. Clark, "Novel TiO_2 CVD films for semiconductor photocatalysis," *Journal of Photochemistry and Photobiology A*, vol. 151, no. 1–3, pp. 171–179, 2002.

[23] H. Jiang and L. Gao, "Enhancing the UV inducing hydrophilicity of TiO_2 thin film by doping Fe ions," *Materials Chemistry and Physics*, vol. 77, no. 3, pp. 878–881, 2002.

[24] M. L. Hitchman and F. Tian, "Studies of TiO_2 thin films prepared by chemical vapour deposition for photocatalytic and photoelectrocatalytic degradation of 4-chlorophenol," *Journal of Electroanalytical Chemistry*, vol. 538-539, pp. 165–172, 2002.

[25] Y. Suda, H. Kawasaki, T. Ueda, and T. Ohshima, "Preparation of high quality nitrogen doped TiO_2 thin film as a photocatalyst using a pulsed laser deposition method," *Thin Solid Films*, vol. 453-454, pp. 162–166, 2004.

[26] J. G. Yu, H. G. Yu, B. Cheng, X. J. Zhao, J. C. Yu, and W. K. Ho, "The effect of calcination temperature on the surface microstructure and photocatalytic activity of TiO_2 thin films prepared by liquid phase deposition," *Journal of Physical Chemistry B*, vol. 107, no. 50, pp. 13871–13879, 2003.

[27] Q. Xiang, J. Yu, and M. Jaroniec, "Tunable photocatalytic selectivity of TiO_2 films consisted of flower-like microspheres with exposed 001 facets," *Chemical Communications*, vol. 47, no. 15, pp. 4532–4534, 2011.

[28] S. K. Zheng, T. M. Wang, C. Wang, and G. Xiang, "Photocatalytic activity study of TiO_2 thin films with and without Fe ion implantation," *Nuclear Instruments and Methods in Physics Research B*, vol. 187, no. 4, pp. 479–484, 2002.

[29] S. K. Zheng, T. M. Wang, W. C. Hao, and R. Shen, "Improvement of photocatalytic activity of TiO_2 thin film by Sn ion implantation," *Vacuum*, vol. 65, no. 2, pp. 155–159, 2002.

[30] B. Z. Rameev, F. Yildiz, L. R. Tagirov, B. Aktaş, W. K. Park, and J. S. Moodera, "ESR study of Co-doped TiO_2 thin films," *Journal of Magnetism and Magnetic Materials*, vol. 258-259, pp. 361–364, 2003.

[31] J. Yu, Q. Xiang, and M. Zhou, "Preparation, characterization and visible-light-driven photocatalytic activity of Fe-doped titania nanorods and first-principles study for electronic structures," *Applied Catalysis B*, vol. 90, no. 3-4, pp. 595–602, 2009.

[32] Z. Xu and J. Yu, "Visible-light-induced photoelectrochemical behaviors of Fe-modified TiO_2 nanotube arrays," *Nanoscale*, vol. 3, no. 8, pp. 3138–3144, 2011.

[33] Y. Li, W. Wlodarski, K. Galatsis et al., "Gas sensing properties of p-type semiconducting Cr-doped TiO_2 thin films," *Sensors and Actuators B*, vol. 83, no. 1–3, pp. 160–163, 2002.

[34] T. Sumita, T. Yamaki, S. Yamamoto, and A. Miyashita, "Photo-induced surface charge separation of highly oriented TiO_2 anatase and rutile thin films," *Applied Surface Science*, vol. 200, no. 1–4, pp. 21–26, 2002.

[35] V. Collins-Martínez, A. L. Ortiz, and A. A. Elguézabal, "Influence of the anatase/rutile ratio on the TiO_2 photocatalytic activity for the photodegradation of light hydrocarbons," *International Journal of Chemical Reactor Engineering*, vol. 5, article A92, 2007.

[36] J. Ryu and W. Choi, "Substrate-specific photocatalytic activities of TiO_2 and multiactivity test for water treatment application," *Environmental Science and Technology*, vol. 42, no. 1, pp. 294–300, 2008.

[37] V. G. Bessergenev, R. J. F. Pereira, and A. M. Botelho do Rego, "Thin film sulphides and oxides of 3d metals prepared from complex precursors by CVD," *Surface and Coatings Technology*, vol. 201, no. 22-23, pp. 9141–9145, 2007.

[38] V. G. Besserguenev, R. J. F. Pereira, M. C. Mateus, I. V. Khmelinskii, R. C. Nicula, and E. Burkel, "TiO_2 thin film synthesis from complex precursors by CVD, its physical and photocatalytic properties," *International Journal of Photoenergy*, vol. 5, no. 2, pp. 99–105, 2003.

[39] V. G. Bessergenev, I. V. Khmelinskii, R. J. F. Pereira, V. V. Krisuk, A. E. Turgambaeva, and I. K. Igumenov, "Preparation of TiO_2 films by CVD method and its electrical, structural and optical properties," *Vacuum*, vol. 64, no. 3-4, pp. 275–279, 2002.

[40] A. A. Gribb and J. F. Banfield, "Particle size effects on transformation kinetics and phase stability in nanocrystalline TiO_2," *American Mineralogist*, vol. 82, no. 7-8, pp. 717–728, 1997.

[41] M. N. Grecu, S. Constantinescu, D. Tărăbăşanu-Mihăilă, D. Ghica, and I. Bibicu, "Spin dynamics in ^{57}Fe-doped TiO_2 anatase nanoparticles," *Physica Status Solidi B*, vol. 248, no. 12, pp. 2927–2931, 2011.

[42] X. Yang, F. Ma, K. Li et al., "Mixed phase titania nanocomposite codoped with metallic silver and vanadium oxide: new efficient photocatalyst for dye degradation," *Journal of Hazardous Materials*, vol. 175, no. 1–3, pp. 429–438, 2010.